arXiv:1608.08602v1 [astro-ph.GA] 30 Aug 2016

Baltic Astronomy, vol. 25, 119–138, 2016

REVEALING THE NETWORK OF PERIODIC ORBITS IN GALAXY MODELS WITH A PROLATE OR AN OBLATE DARK MATTER HALO COMPONENT

Euaggelos E. Zotos

Department of Physics, School of Science, Aristotle University of Thessaloniki, GR-541 24, Thessaloniki, Greece; e-mail: evzotos@physics.auth.gr

Received: 2015 April 27; accepted: 2015 June 23

Abstract. Locating the position of periodic orbits in galaxies is undoubtedly an issue of paramount importance. We reveal the position and the stability of periodic orbits of stars moving in the meridional plane (R, z) of an axially symmetric galactic model with a disk, a spherical nucleus, and a biaxial dark matter halo component. In particular, we study how all the involved parameters of the dynamical system influence the position and the stability of all resonant families. To locate the position and measure the stability of periodic orbits we use a highly sensitive numerical code which is able to identify resonant periodic orbits of the type $n : m$. Two cases are studied for every parameter: (i) the case where the dark matter halo component is prolate and (ii) the case where an oblate dark matter halo is present. Our numerical exploration reveals that all the dynamical quantities affect, more or less, the position and the stability of the periodic orbits. It is shown that the mass of the nucleus, the mass of the disk, the halo flattening parameter, the scale length of the halo, the angular momentum, and the total orbital energy are the most influential quantities, while the effect of all other parameters is much weaker.

Key words: galaxies: kinematics and dynamics – structure – periodic orbits

1. INTRODUCTION

Periodic orbits undoubtedly play an important role in the analysis of various types of dynamical systems. Indeed, in dynamical systems with strong chaotic behavior, unstable periodic orbits create a "skeleton" for chaotic trajectories (Cvitanović 1991). Furthermore, a well regarded definition of chaos (Devaney 1989) requires the existence of an infinite number of unstable periodic orbits that are dense in the chaotic set.

Several geometric and dynamical properties of chaotic sets, such as Lyapunov exponents, fractal dimensions, entropies (Ott 1993), can be determined from the location and the stability properties of the embedded periodic orbits. Periodic orbits are central to understanding of quantum-mechanical properties of non-separable systems: the energy level density of such systems can be expressed in a semiclassical approximation as a sum over the unstable periodic orbits of the corresponding

classical system (Gutzwiller 1990). Topological description of a chaotic attractor also benefits from the knowledge of periodic orbits. For example, a large set of periodic orbits is highly constraining to the symbolic dynamics and can be used to extract the location of a generating partition (Davidchack et al. 2000; Plumecoq & Lefranc 2000). The significance of periodic orbits for the experimental study of dynamical systems has been demonstrated in a wide variety of systems (Lathrop & Kostelich 1989), especially for the purpose of controlling chaotic dynamics (Ott et al. 1990) with possible application in communication (Bollt et al. 1997). In a Hamiltonian system, periodic orbits are not usually isolated but form one-parametric families. Naturally, the value of the Hamiltonian function plays the role of the parameter. Thus even in the case when the original Hamiltonian does not explicitly contain any parameter, it is possible to observe bifurcations of periodic orbits. A bifurcation corresponds to a resonance between the frequency of a periodic orbit and the frequency of small oscillations around it. In a generic situation there is a family of hyperbolic periodic orbits of a multiple period, which shrinks to the resonant periodic orbit at an exact resonance. Separatrices of the hyperbolic periodic orbit have to intersect due to Hamiltonian nature of the problem. Segments of separatrices of the corresponding resonant normal form make up a closed loop around the periodic trajectory.

In an effort to understand the structure of the solutions of non-integrable dynamical systems, the numerical determination of their periodic solutions and their stability properties plays a role of fundamental importance. The fact that for most dynamical systems the periodic orbits are dense in the set of all possible solutions, at least in certain parts of the phase space, necessitates the presence of an efficient numerical method for their determination. Over the last decades, several works developing different numerical algorithms in order to compute periodic orbits have been presented. Abalakin (1961, 1963) in pioneer works examined in detail nearly circular periodic orbits inside a heterogeneous ellipsoid for two particular cases regarding the density distribution. Furthermore, Antonov (1974) developed a topological method of finding periodic orbits. Later on, Prendergast proposed a method to find approximate solutions of the Hamiltonian equations of motion in the form of rational formulae. Prendergast (1982) and Wood (1984) applied this method to Hamiltonian systems with one and two degrees of freedom, while Contopoulos & Seimenis (1990) deployed the same method to the logarithmic potential in order to obtain the families of periodic orbits. The use of differential correction algorithms for the numerical computation of either two- or three-dimensional periodic orbits is not a new result. The contributions of Deprit & Henrard (1967) and Henrard & Lemaitre (1986) with respect to the systems with two degrees of freedom, and Belbruno et al. (1994), Contopoulos & Barbanis (1985), Howell (1984), Karimov & Sokolsky (1989), Lara & Paláez (2002) and Scheeres (1999) with respect to the systems with three degrees of freedom, can be mentioned. Usually, a dynamical system admits some kind of symmetry, and, consequently, the traditional approaches used for computing periodic orbits were based on those symmetries. However, when dealing with force fields without symmetries, a different approach must be used. The normal procedure is then the application of the Poincaré map, and differential corrections are obtained through the computation of the state transition matrix along the periodic orbit. On the other hand, for conservative systems the monodromy matrix has one unit eigenvalue with multiplicity two related to the time invariance of the system thus preventing the computation of the corrections. Two approaches are normally used

to compute the nontrivial eigenvalues, both of them based on the integration of the variations in Cartesian coordinates. The first computes the complete state transition matrix and uses basic techniques of matrix algebra for obtaining the eigenvalues of a singular matrix. The second eliminates the two unit eigenvalues from the system by creating a lower dimensional map. In a recent paper by Zotos (2014) (hereafter Paper I) we introduced a composite analytic, axially symmetric galactic gravitational model that embraces the general features of a disk galaxy with a dense massive nucleus and a biaxial prolate or oblate dark matter halo component. Then we distinguished between regular and chaotic motion of stars moving in the meridional (R, z) plane and we also performed an orbit classification by separating regular orbits into different regular families. In the present paper we use the same galactic model in an attempt to reveal the complete network of periodic orbits.

This paper is organized as follows. In Section 2, we present in detail the structure and the properties of the gravitational galactic model. In Section 3, we describe some theoretical and computational details of our methods. In the following section, we investigate how all the involved parameters of the dynamical system influence the position and the stability of the periodic orbits when a prolate or an oblate dark halo component is present. Our paper ends with Section 5, where the discussion and the conclusions of this research are presented.

2. PRESENTATION OF THE GALACTIC MODEL

Let us briefly recall the galactic gravitational model which was introduced in Paper I. The total potential $V(R, z)$ consists of three components: a spherical nucleus, a disk, and a biaxial dark matter halo component.

For the description of the nucleus, we use the Plummer potential (e.g., Binney & Tremaine 2008):

$$V_{\rm n}(R,z) = \frac{-GM_{\rm n}}{\sqrt{R^2+z^2+c_{\rm n}^2}}. \tag{1}$$

Here, G is the gravitational constant, while $M_{\rm n}$ and $c_{\rm n}$ are the mass and the scale length of the nucleus, respectively. At this point, we must clarify that we do not include any relativistic effects, because the nucleus represents a bulge rather than a black hole or any other compact object.

The galactic disk is represented by a generalization of the Miyamoto & Nagai (1975) potential (see also Carlberg & Innanen 1987)

$$V_{\rm d}(R,z) = \frac{-GM_{\rm d}}{\sqrt{b^2+R^2+\left(\alpha+\sqrt{h^2+z^2}\right)^2}}, \tag{2}$$

where $M_{\rm d}$ is the mass of the disk, b is the core radius of the disk-halo, α is the scale length of the disk, while h corresponds to the disk scale height.

The potential of the dark matter halo is modeled by the flattened axisymmetric logarithmic potential

$$V_{\rm h}(R,z) = \frac{\upsilon_0^2}{2}\ln\left(R^2+\beta z^2+c_{\rm h}^2\right), \tag{3}$$

where β is the flattening parameter and $c_{\rm h}$ stands for the scale length of the dark halo component. The parameter υ_0 is used for the consistency of the galactic

units. This potential can model a wide variety of shapes of galactic haloes by suitably choosing the parameter β. In particular, when $0.1 \leq \beta < 1$, the dark matter halo is prolate, when $\beta = 1$ it is spherical and when $1 < \beta < 2$ it is oblate. In this work, we use a system of galactic units where the unit of length is 1 kpc, the unit of velocity is 10 km s^{-1}, and $G = 1$. Thus, the unit of mass is $2.325 \times 10^7 M_\odot$, that of time is 0.9778×10^8 yr, the unit of angular momentum (per unit mass) is 10 km kpc^{-1} s^{-1}, and the unit of energy (per unit mass) is 100 km^2 s^{-2}. Our main objective is to investigate the regular or chaotic nature of orbits in two different cases: when the dark matter halo component is (i) prolate (PH model) and (ii) oblate (OH model). Our models have the following standard values of the parameters: $M_\mathrm{d} = 7000$ (corresponding to 1.63×10^{11} $M_\odot$, i.e., a normal disk galaxy mass), $b = 6$, $\alpha = 3$, $h = 0.2$, $M_\mathrm{n} = 250$ (corresponding to $5.8 \times 10^9 M_\odot$), $c_\mathrm{n} = 0.25$, $\upsilon_0 = 20$ and $c_\mathrm{h} = 8.5$, while $\beta = 0.5$ for the PH model and $\beta = 1.5$ for the OH model. The values for the disk and the nucleus were chosen with a Milky Way-type galaxy in mind (e.g., Allen & Santillán 1991). In the case of the prolate dark halo, the set of the values of the parameters defines the standard prolate model (SPM), while when the dark halo is oblate, we use the standard oblate model (SOM). Here, we must point out that our gravitational potential is truncated ar $R_\mathrm{max} = 50$ kpc, otherwise the total mass of the galaxy modeled by this potential would be infinite, which is obviously not physical. The values of the parameters of the standard models secure positive density inside the region with $R \leq 50$ kpc[1].

Taking into account that the total potential $V(R, z)$ is axisymmetric, the z-component of the angular momentum (L_z) is conserved. With this restriction, orbits can be described by means of the effective potential (e.g., Binney & Tremaine 2008)

$$V_\mathrm{eff}(R, z) = V(R, z) + \frac{L_z^2}{2R^2}. \tag{4}$$

The Hamiltonian to the effective potential given in Eq. (4) can be written as

$$H = \frac{1}{2}\left(\dot{R}^2 + \dot{z}^2\right) + V_\mathrm{eff}(R, z) = E, \tag{5}$$

where $\dot{R}$ and $\dot{z}$ are momenta per unit mass, and conjugate to R and z, respectively, while E is the numerical value of the Hamiltonian, which is conserved. Therefore, an orbit is restricted to the permissible area in the meridional plane satisfying $E \geq V_\mathrm{eff}$.

Consequently, the corresponding equations of motion in the meridional plane are

$$\begin{aligned} \ddot{R} &= -\frac{\partial V_\mathrm{eff}}{\partial R}, \\ \ddot{z} &= -\frac{\partial V_\mathrm{eff}}{\partial z}, \end{aligned} \tag{6}$$

[1] The density of the model will be negative at large enough distances from the center ($R > 50$ kpc), and this is a general property of all models with ellipsoidal (but non-spherical) equipotentials.

where a double dot indicates a derivative with respect to time.

3. THEORETICAL AND COMPUTATIONAL DETAILS

For the location of the position and the measurement of the stability of periodic orbits we use a highly sensitive numerical code which is able to identify resonant periodic orbits of the type $n : m$. The $n : m$ notation we use for the resonant periodic orbits is according to Carpintero & Aguilar (1998) and Zotos & Carpintero (2013), where the ratio of those integers corresponds to the ratio of the main frequencies of the orbit, where main frequency is the frequency of greatest amplitude in each coordinate. Main amplitudes, when having a rational ratio, define the resonances of an orbit. Initially we define for every variable parameter an interval of realistic values. The numerical code begins from the value corresponding to the standard model (SPM and SOM), which is always somewhere inside the main interval, and then, using a variable step, scans all the available interval thus calculating the entire resonant family. In order to check the robustness and efficiency of our numerical algorithm, we recalculated some of the halo orbits of the classical restricted three-body problem (R3BP) presented initially in Gómez et al. (1985). All the performed tests indicated a satisfactory agreement with the corresponding numerical outcomes for either stability index of the period of the periodic orbits.

The equations of motion are solved for a given value of the Hamiltonian, starting with initial conditions $(R_0, z_0, \dot{R}_0, \dot{z_0})$ in the plane $z = 0$, for $\dot{z} > 0$. The next intersection with the $z = 0$ plane with $\dot{z} > 0$ is found and the exact initial conditions for the periodic orbit are calculated using a Newton iterative method. A periodic orbit is found when the initial and final coordinates coincide with an accuracy of at least 10^{-12}.

The estimation of the linear stability of a periodic orbit is based on the theory of variational equations. We first consider small deviations from its initial conditions, and then integrate the orbit again to the next upward intersection. Let the variational equations of a specific periodic orbit of period T be

$$\dot{\xi}_i(t) = \sum_{j=1}^{4} \frac{\partial F_i}{\partial x_j} \xi_j \qquad (i, j = 1, 2, 3, 4). \tag{7}$$

If $X(t)$ is the matrix, whose columns are the four solutions of the system (7) with initial conditions (1,0,0,0), (0,1,0,0), (0,0,1,0) and (0,0,0,1), then we have the so-called monodromy matrix

$$X(t) = \begin{pmatrix} \frac{\partial R}{\partial R_0} & \frac{\partial R}{\partial z_0} & \frac{\partial R}{\partial \dot{R}_0} & \frac{\partial R}{\partial \dot{z}_0} \\ \frac{\partial z}{\partial R_0} & \frac{\partial z}{\partial z_0} & \frac{\partial z}{\partial \dot{R}_0} & \frac{\partial z}{\partial \dot{z}_0} \\ \frac{\partial \dot{R}}{\partial R_0} & \frac{\partial \dot{R}}{\partial z_0} & \frac{\partial \dot{R}}{\partial \dot{R}_0} & \frac{\partial \dot{R}}{\partial \dot{z}_0} \\ \frac{\partial \dot{z}}{\partial R_0} & \frac{\partial \dot{z}}{\partial z_0} & \frac{\partial \dot{z}}{\partial \dot{R}_0} & \frac{\partial \dot{z}}{\partial \dot{z}_0} \end{pmatrix}. \tag{8}$$

When $t = T$, there is also a monodromy matrix $X(T)$. The stability of a periodic orbit depends on the eigenvalues of this monodromy matrix. We define

the stability index (S.I.) as

$$\text{S.I.} = \text{Tr}(\text{X(T)}) - 2, \tag{9}$$

where $\text{Tr}(\text{X(T)}) = \lambda_1 + \lambda_2 + \lambda_3 + \lambda_4$ is the trace of the monodromy matrix, while λ_i $(i = 1, 4)$ are the eigenvalues. Now, according to the value of S.I. we can determine if a periodic orbit is stable or unstable. In particular, if $|\text{S.I.}| < 2$ the periodic orbit is stable, if $|\text{S.I.}| > 2$ the periodic orbit is unstable, while if $|\text{S.I.}| = 2$ the periodic orbit is critically stable.

For each initial condition of a periodic orbit, we integrated the equations of motion (6), as well as the variational equations (7), using a double precision Bulirsch-Stoer algorithm (e.g., Press et al. 1992) with a small time step of the order of 10^{-2}, which is sufficient enough for the desired accuracy of our computations (i.e., our results practically do not change by halving the time step). Here we should emphasize, as our previous numerical experience suggests, that the Bulirsch-Stoer integrator is both faster and more accurate than a double precision Runge-Kutta-Fehlberg algorithm of order 7 with the Cash-Karp coefficients. In all cases, the energy integral (Eq. 5) was conserved better than one part in 10^{-11}, although for most orbits it was better than one part in 10^{-12}.

4. THE NETWORK OF PERIODIC ORBITS

In all cases, the energy was set to 600 and the angular momentum of the orbits is $L_z = 10$. We chose, for both PH and OH models, the particular energy level, which yields $R_{\max} \simeq 15$ kpc, where $R_{\max}$ is the maximum possible value of R on the $(R, \dot{R})$ phase plane. In every case, we let only one quantity vary in a predefined range, while fixing the values of all the other parameters, according to SPM and SOM. Once the values of the parameters were chosen, the numerical code begins locating the position and computing the corresponding stability index of periodic orbits along the predefined range of values. The step between two successive values of a variable quantity is chosen in such a way that every resonant family contains at least 5000 initial conditions $(R_0, \dot{R}_0)$ of periodic orbits with $z_0 = 0$, while $\dot{z_0}$ is always obtained from the energy integral (Eq. 5).

Our numerical calculations indicate that in the PH models there are six main resonant families: (i) 2:1 banana-type orbits; (ii) 1:1 open linear orbits; (iii) 4:3 resonant orbits; (iv) 6:3 resonant orbits; (v) 10:5 resonant orbits; (vi) 12:7 resonant orbits. In addition, in the OH models there are only five main resonant families: (i) 2:1 banana-type orbits; (ii) 1:1 open linear orbits; (iii) 3:2 resonant orbits; (iv) 4:3 resonant orbits; (v) 8:5 resonant orbits. In Table 1 of Paper I we provide the types and the exact initial conditions of the main orbital families for the SPM and SOM, while in Figs. 6 and 7 of Paper I we depict the shapes of these resonant periodic orbits.

In every case we present a very informative diagram, the so-called "characteristic" orbital diagram (Contopoulos & Mertzanides 1977). It shows the evolution of the R coordinate of the initial conditions of the periodic orbits of each orbital family as a function of the value of the variable quantity. Here we should emphasize that, for periodic orbits starting perpendicular to the R-axis, we need only the initial condition of R_0 in order to locate them on the characteristic diagram. On the other hand, for orbits not starting perpendicular to the R-axis, initial conditions as position-velocity pairs $(R, \dot{R})$ are required and, therefore, the

characteristic diagram is now three-dimensional providing the full information regarding the interrelations of the initial conditions in a tree of families of periodic orbits. In the following two-dimensional characteristic diagrams we will see that some resonant families cross one another. Here it should be clarified that the full characteristic curves of some resonant families (i.e., 1:1, the 3:2 and 6:3) are three-dimensional since $\dot{R}_0 \neq 0$, however we decided to combine all families together in a two-dimensional plot containing only the evolution of the R coordinate (of course, in the 3D $(R, \dot{R}, M_{\rm n})$ space the corresponding characteristic curves do not cross one another). Furthermore, we provide the so-called "stability diagram" (Contopoulos & Barbanis 1985; Contopoulos & Magnenat 1985) which illustrates the stability of all the families of periodic orbits in our dynamical system when the numerical value of the variable quantity varies, while all the other parameters remain constant. A periodic orbit is stable if only the stability index (S.I.) (Zotos 2013) is between –2 and +2. This diagram helps us monitor the evolution of S.I. of the resonant periodic orbits as well as the transitions from stability to instability and vice versa.

4.1. Influence of the mass of the nucleus

To study how the mass of the nucleus, $M_{\rm n}$, influences the position and stability of periodic orbits, we let it vary while fixing all the other parameters of our model, and integrate orbits in the meridional plane for the set $M_{\rm n} = \{0, 50, 100, ..., 500\}$. In all cases, the energy was set to 600 and the angular momentum of the orbits $L_z = 10$. Once the values of the parameters were chosen, we computed a set of initial conditions as described in Sec. 3, and integrated the corresponding orbits.

The evolution of the R coordinate of the periodic orbits as $M_{\rm n}$ varies for the PH models is shown in Fig. 1a. The black solid lines indicate the borders of the limiting curves. It can be seen that the main families of periodic orbits (i.e., the 2:1, 1:1, 4:3 and 10:5 families) are present throughout the entire range of values of $M_{\rm n}$. On the other hand, some secondary resonances (i.e., the 6:3 and 12:7 families) terminate earlier than the range of values. In particular, our numerical calculations shown in Fig. 1b reveal that the 6:3 family is unstable for $371 \leq M_{\rm n} \leq 386$, while the 12:7 family is unstable for $272 \leq M_{\rm n} \leq 344$. Looking carefully at the stability diagram of Fig. 1b we observe that the 1:1 family becomes unstable near the lower and upper limits of the range. Specifically the 1:1 resonant family is unstable for $0 \leq M_{\rm n} \leq 23.8$ and for $457 \leq M_{\rm n} \leq 500$. We also see that the 2:1 resonant family spends most of its life near the upper stability limit (+2), however it never crosses it. Similarly in Fig. 1c we present the evolution of the R coordinate of the periodic orbits as a function of $M_{\rm n}$ for the OH models. Here the only resonant family, that terminates earlier at relatively high values of the mass of the nucleus, is the 8:5 family. In particular this family terminates at $M_{\rm n} = 395.2$ without exhibiting any instability first.

4.2. Influence of the scale length of the nucleus

Now we proceed to investigate how the scale length of the nucleus $c_{\rm n}$ influences the position and stability of the periodic orbits in our PH and OH models. Again, we let it vary while fixing all the other parameters of our galactic model and integrating orbits in the meridional plane for the set $c_{\rm n} = \{0.05, 0.10, 0.15, ..., 0.50\}$.

The evolution of the R coordinate of the periodic orbits as $c_{\rm n}$ varies for the PH models is shown in Fig. 2a. It is evident that the scale length of the nucleus

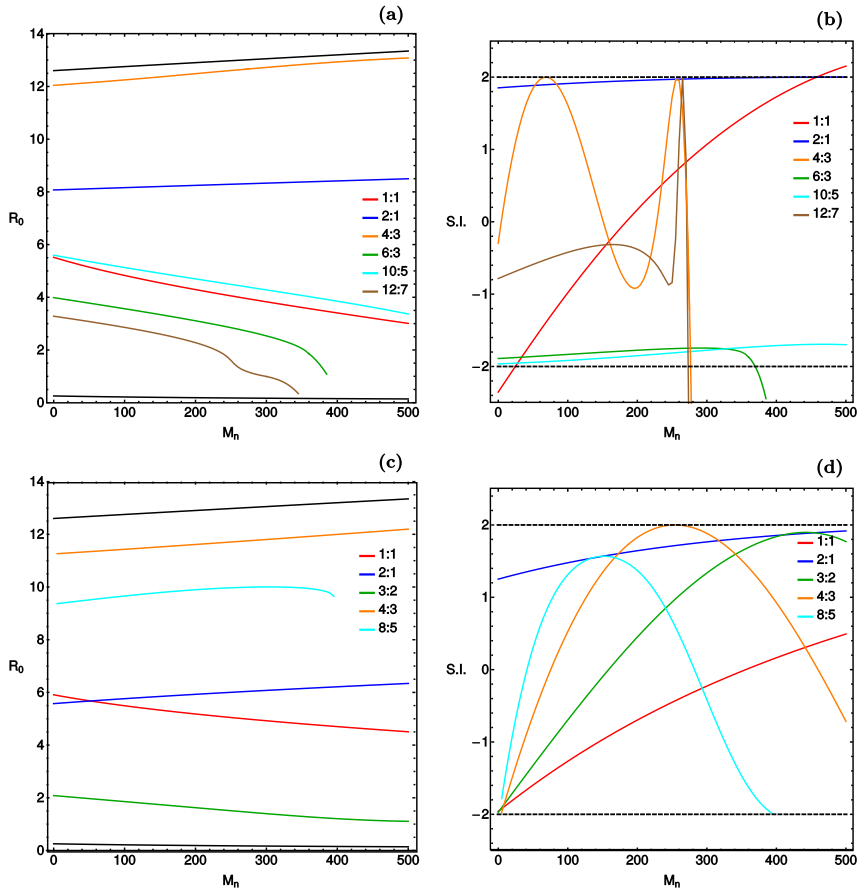

Fig. 1. Evolution of the R coordinate of periodic orbits as a function of mass of the nucleus, $M_{\rm n}$, for the PH models (panel a) and OH models (panel c), and the evolution of the stability index S.I. as a function of $M_{\rm n}$ for the PH models (panel b) and OH models (panel d).

influences very weakly the position of the periodic orbits in the PH models. For this reason all the resonant families survive the entire range of values of $c_{\rm n}$. The corresponding stability diagram shown in Fig. 2b informs us that the 4:3 resonant family is unstable for $0.05 \leq c_{\rm n} \leq 0.134$, while the 12:7 resonant family is unstable for $0.05 \leq c_{\rm n} \leq 0.147$. Things are quite similar for the OH models. Indeed, the characteristic diagram of Fig. 2c shows once more that the scale length of the nucleus hardly affects the position of the periodic orbits which, according to Fig. 2d, all remain stable throughout the entire range of values of $c_{\rm n}$. It should be noticed that the stability index of the 4:3 resonant family evolves almost parallel to the upper stability limit (+2), but never crosses it.

4.3. Influence of the mass of the disk

Our next step is to reveal how the position and stability of periodic orbits in our PH and OH models are affected by the mass of the disk $M_{\rm d}$. As usual, we

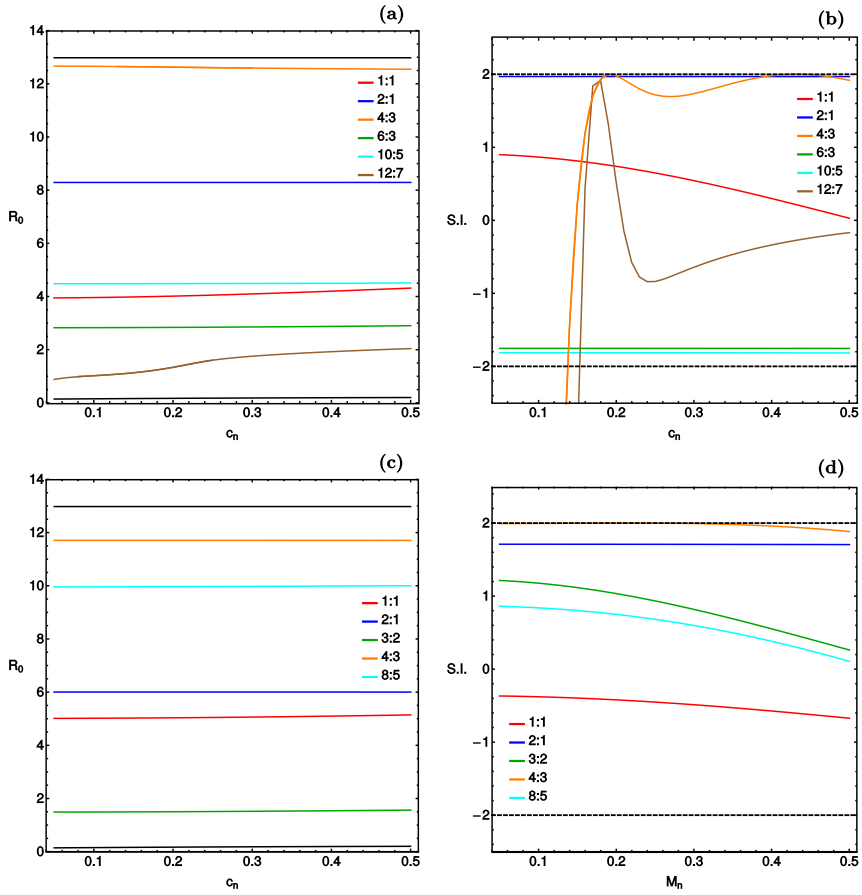

Fig. 2. Evolution of the R coordinate of periodic orbits as a function of the scale length of the nucleus, $c_{\rm n}$, for the PH models (panel a) and OH models (panel c), and the evolution of the stability index S.I. as a function of $c_{\rm n}$ for the PH models (panel b) and OH models (panel d).

let this quantity vary while fixing the values of all the other parameters of our galactic model and integrating orbits in the meridional plane for the set $M_{\rm d} = \{4500, 5000, 5500, ..., 9000\}$.

Fig. 3a shows the evolution of the R coordinate of periodic orbits as a function of the mass of the disk for the PH models. We observe an almost linear relocation of the position of the periodic orbits. The corresponding stability diagram of Fig. 3b reveals that the 4:3 resonant family is unstable for $4500 \leq M_{\rm d} \leq 6218$, while the 12:7 resonant family is unstable for $5248 \leq M_{\rm d} \leq 6295$ and terminates at $M_{\rm d} = 5248$. Furthermore, we see that the 2:1 resonant family for about $M_{\rm d} > 6800$ becomes almost critically stable. The evolution of the R coordinate of the periodic orbits as a function of the mass of the disk for the OH models is shown in Fig. 3c. One can observe that all resonant families are present throughout the entire range of the values of $M_{\rm d}$, while the corresponding stability diagram of Fig. 3d indicates that all resonant families are stable.

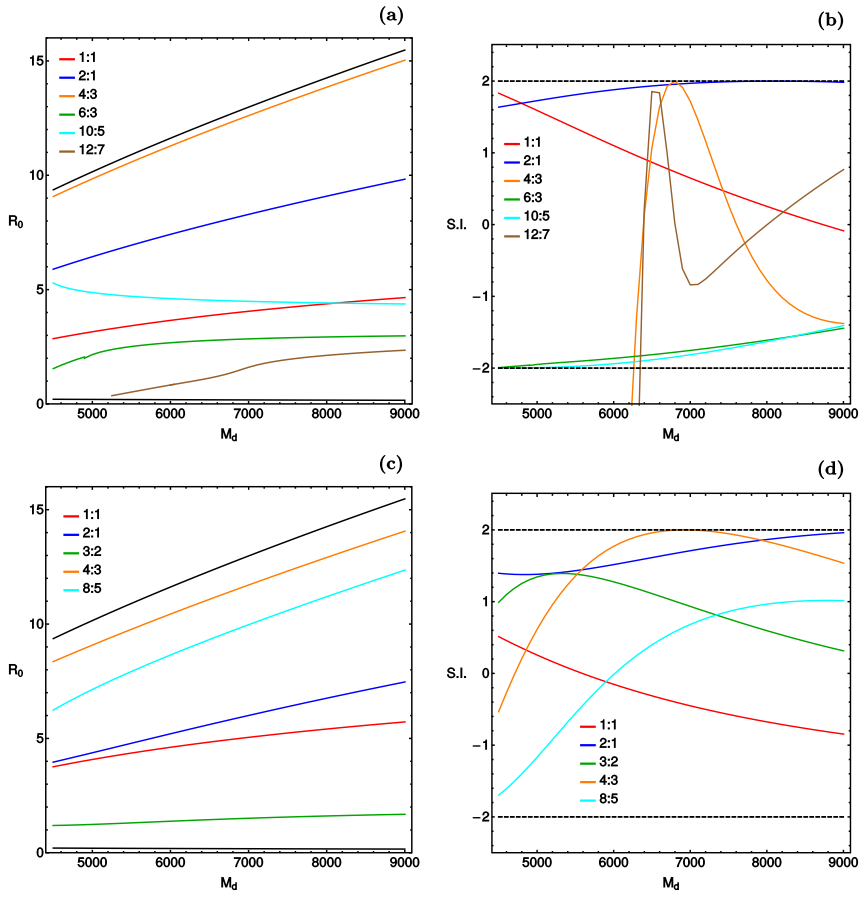

Fig. 3. Evolution of the R coordinate of periodic orbits as a function of the mass of the disk, $M_{\rm d}$, for the PH models (panel a) and OH models (panel c), and the evolution of the stability index S.I. as a function of $M_{\rm d}$ for the PH models (panel b) and OH models (panel d).

4.4. Influence of the core radius of the disk-halo

The next parameter under investigation is the core radius of the disk-halo, b. We will try to understand how the position and the stability of the periodic orbits in our PH and OH galaxy models are influenced by b. Again, we let this quantity vary while fixing the values of all the other parameters of our galactic model and integrating orbits in the meridional plane for the set $b = \{4, 4.5, 5, ..., 8\}$.

The evolution of the position of periodic orbits as a function of the core radius of the disk-halo for the PH models is given in Fig. 4a. It is interesting to notice that for $b = 8$ the 10:5 secondary resonant family almost bifurcates from the main parent 2:1 resonant family. In addition, the corresponding stability diagram shown in Fig. 4b indicates that the 4:3 resonant family becomes unstable for $6.58 \leq b \leq 8$, while the 12:7 resonant family is unstable for $4 \leq b \leq 4.94$. In the same vein we present in Fig. 4c the evolution of the R coordinates of periodic orbits of the OH models as a function of b. Here the vast majority of the computed periodic orbits

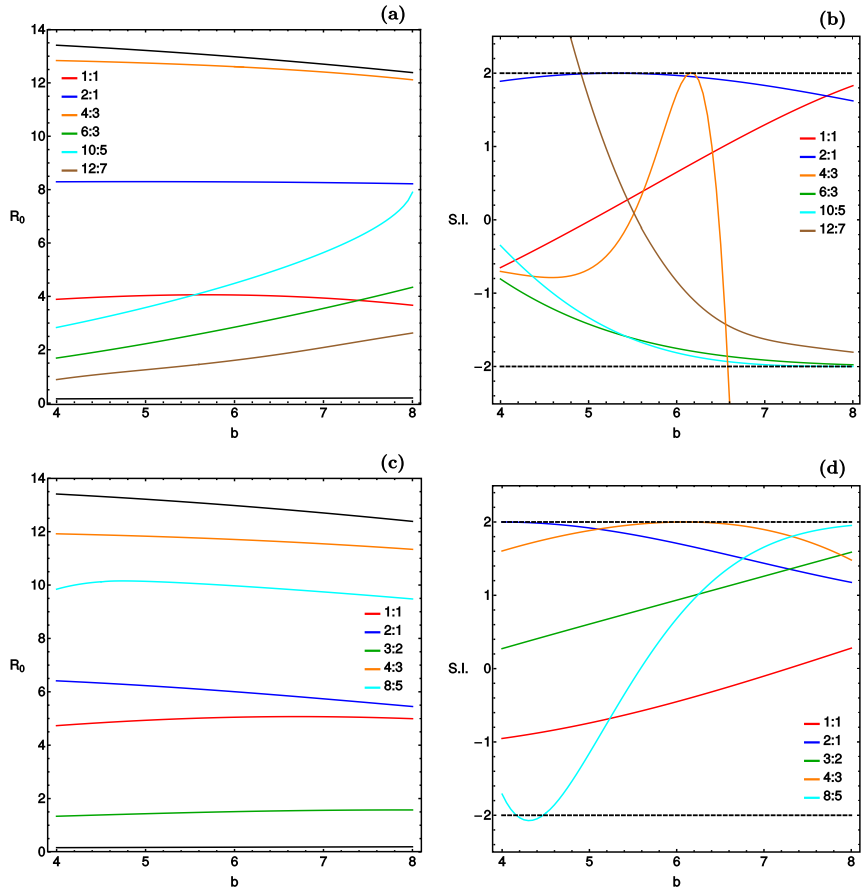

Fig. 4. Evolution of the R coordinate of periodic orbits as a function of the core radius of the disk-halo, b, for the PH models (panel a) and OH models (panel c), and the evolution of the stability index S.I. as a function of b for the PH models (panel b) and OH models (panel d).

are stable, while only the 8:5 resonant family displays a small branch of unstable periodic orbits. Looking at Fig. 4d we see that this branch is located near the lower boundary of the family and specifically for $4.21 \leq b \leq 4.46$.

4.5. Influence of the scale length of the disk

We continue our quest trying to understand how the scale length of a galaxy, α, influences the position and the stability of periodic orbits in our PH and OH galaxy models. As usual, we let this parameter vary while fixing the values of all the other quantities of our galactic model and integrating orbits in the meridional plane for the set $\alpha = \{2.5, 2.75, 3, ..., 5\}$.

The following Fig. 5a shows the evolution of the R coordinate of periodic orbits as a function of the scale length of the disk for the PH models. We observe that the only resonant family that terminates earlier is the 12:7 family. In particular, according to the corresponding stability diagram of Fig. 5b this family first becomes

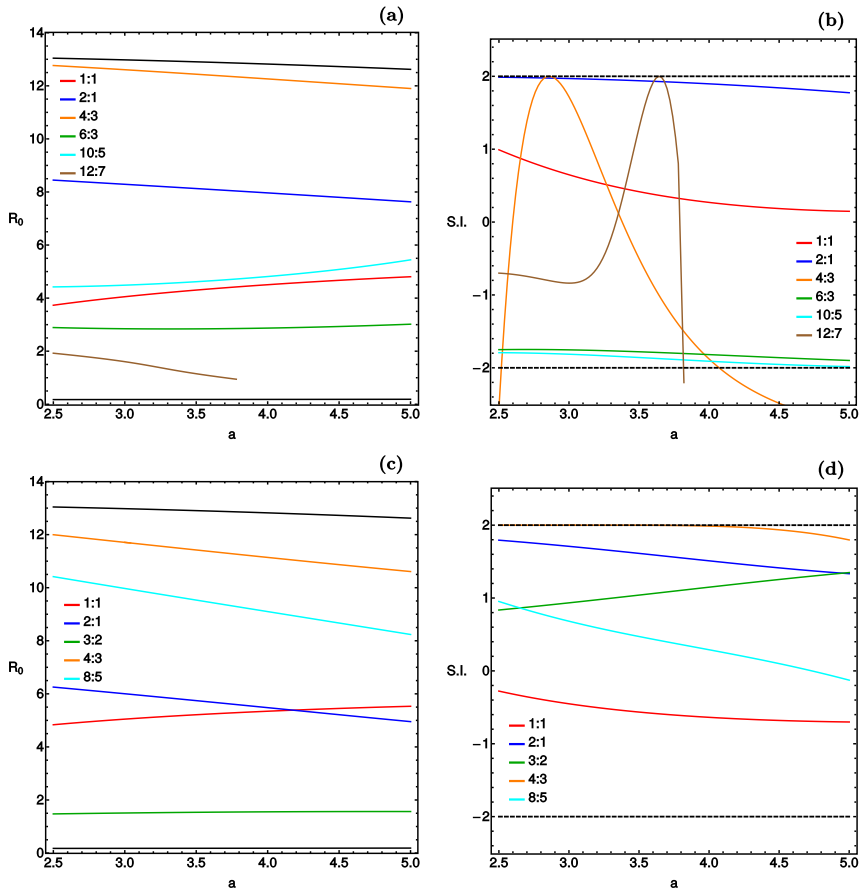

Fig. 5. Evolution of the R coordinate of periodic orbits as a function of the scale length of the disk, α, for the PH models (panel a) and OH models (panel c), and the evolution of the stability index S.I. as a function of α for the PH models (panel b) and OH models (panel d).

unstable for $3.79 \leq \alpha \leq 3.82$ and then it terminates. Moreover, the 4:3 resonant family is also unstable in the intervals $2.5 \leq \alpha \leq 2.52$ and $4.07 \leq \alpha \leq 5$. The evolution of the position of all resonant families of periodic orbits as a function of α for the OH models is given in Fig. 5c. The corresponding stability diagram of Fig. 5d suggests that all resonant families are stable, while only the 4:3 family is almost critically stable in the interval $2.5 \leq \alpha < 4.4$.

4.6. Influence of the scale height of the disk

The next stop of our investigation is to determine how the position and the stability of periodic orbits in our PH and OH galaxy models are affected by the scale height of the disk, h. Following the usual procedure, we let this parameter vary while fixing the values of all the other quantities of our galactic models and integrating orbits in the meridional plane for the set $h = \{0.1, 0.2, 0.3, ..., 1\}$.

The evolution of the position of periodic orbits as a function of the scale height

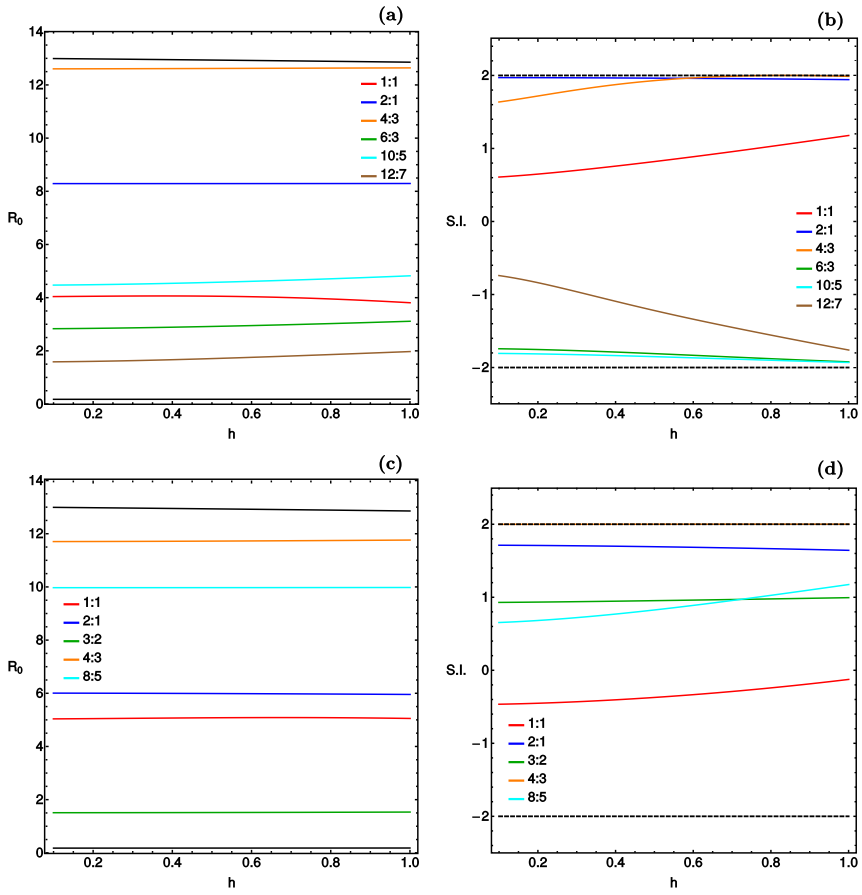

Fig. 6. Evolution of the R coordinate of periodic orbits as a function of the scale height of the disk, h, for the PH models (panel a) and OH models (panel c), and the evolution of the stability index S.I. as a function of h for the PH models (panel b) and OH models (panel d).

of the disk for the PH and OH models is given in Figs. 6a and 6c, respectively. We observe that all the characteristic curves are monotone straight lines, implying that the scale height of the disk practically does not influence the position of the resonant periodic orbits. The corresponding stability diagrams shown in Figs. 6b and 6d indicate that all resonant families are stable except for the 4:3 family which is almost critically stable in most parts of the investigated interval.

4.7. Influence of the halo flattening parameter

The exact shape (prolate, spherical, or oblate) of the dark matter halo is determined by the flattening parameter β. Thus, it would be of particular interest to define how this parameter influences the position and the stability of the periodic orbits in our PH and OH galaxy models. We let this parameter vary while fixing the values of all the other parameters of our galactic models and integrating orbits in the meridional plane for the set $\beta = \{0.1, 0.2, 0.3, ..., 1.9\}$.

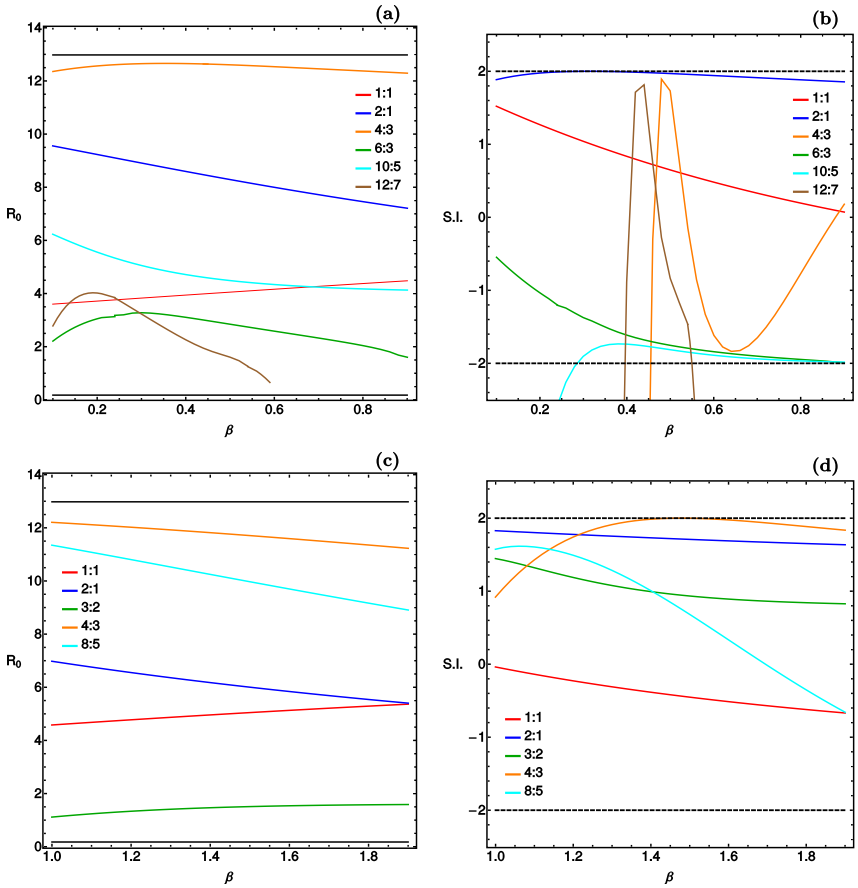

Fig. 7. Evolution of the R coordinate of periodic orbits as a function of the halo flattening parameter β for the PH models (panel a) and OH models (panel c), and the evolution of the stability index S.I. as function of β for the PH models (panel b) and OH models (panel d).

Fig. 7a shows the evolution of the positions of periodic orbits as a function of the halo flattening parameter for the PH models, while the stability of the same families in given in Fig. 7b. We observe that the 4:3 resonant family is unstable for $0.1 \leq \beta \leq 0.446$, while the 10:5 secondary resonant family becomes unstable in the interval $0.1 \leq \beta \leq 0.281$. Furthermore, the 12:7 resonant family is unstable for $0.1 \leq \beta \leq 0.387$ and also for $0.538 \leq \beta \leq 0.592$, while it terminates at $\beta = 0.592$. The evolution of the R coordinate of periodic orbits as a function of β is shown in panel (c). The corresponding stability diagram in panel (d) suggests that all resonant families are stable except for the 4:3 family which is almost critically stable for about $1.35 < \beta < 1.7$.

4.8. Influence of the scale length of the halo

The concentration of the logarithmic, flattened dark matter halo is controlled by its scale length $c_{\rm h}$. In the following, we try to reveal how the scale length of the dark halo influences the position and the stability in our PH and OH galaxy

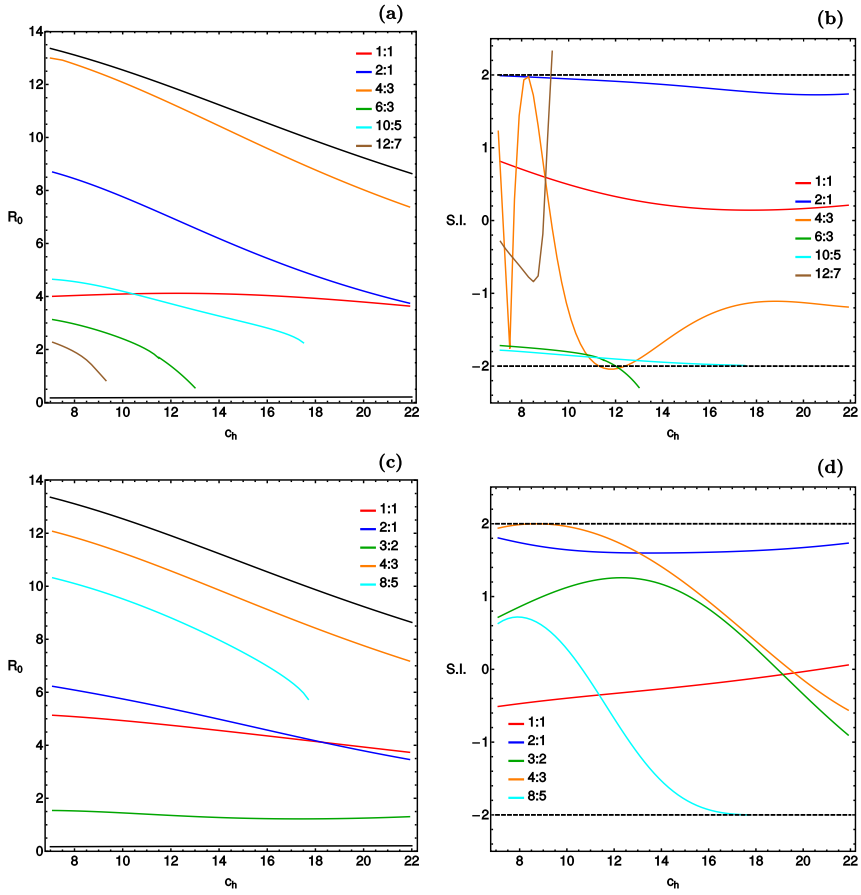

Fig. 8. Evolution of the R coordinate of periodic orbits as a function of the scale length of the halo, $c_{\rm h}$, for the PH models (panel a) and OH models (panel c), and the evolution of the stability index S.I. as a function of $c_{\rm h}$ for the PH models (panel b) and OH models (panel d).

models. We let this parameter vary while fixing the values of all other parameters of our galactic models and integrating orbits in the meridional plane for the set $c_{\rm h} = \{7, 8.5, 10, ..., 22\}$.

The evolution of the R coordinate of periodic orbits as a function of the scale length of the dark matter halo for the PH models is given in Fig. 8a. The corresponding stability diagram (panel b) reveals that the 4:3 resonant family is unstable for $11.29 \leq c_{\rm h} \leq 12.35$, while the 6:3 resonant family becomes unstable for $12.07 \leq c_{\rm h} \leq 13.02$ and terminates at $c_{\rm h} = 13.02$. Moreover, the 10:5 resonant family terminates at $c_{\rm h} = 17.51$ without first exhibiting any signs of instability. On the other hand, the 12:7 resonant family becomes unstable in the interval $8.98 \leq c_{\rm h} \leq 9.25$ and terminates at $c_{\rm h} = 9.25$. Similarly, panel (c) shows the evolution of the position of periodic orbits as a function of $c_{\rm h}$ for the OH models. The stability of the resonant families is illustrated in panel (d), where we can see that all families are stable, while the 4:3 resonant family is almost critically

stable for about $7 < c_{\rm h} < 9.5$. Furthermore, the 8:5 resonant family terminates at $c_{\rm h} = 17.72$ without showing first any unstable branch.

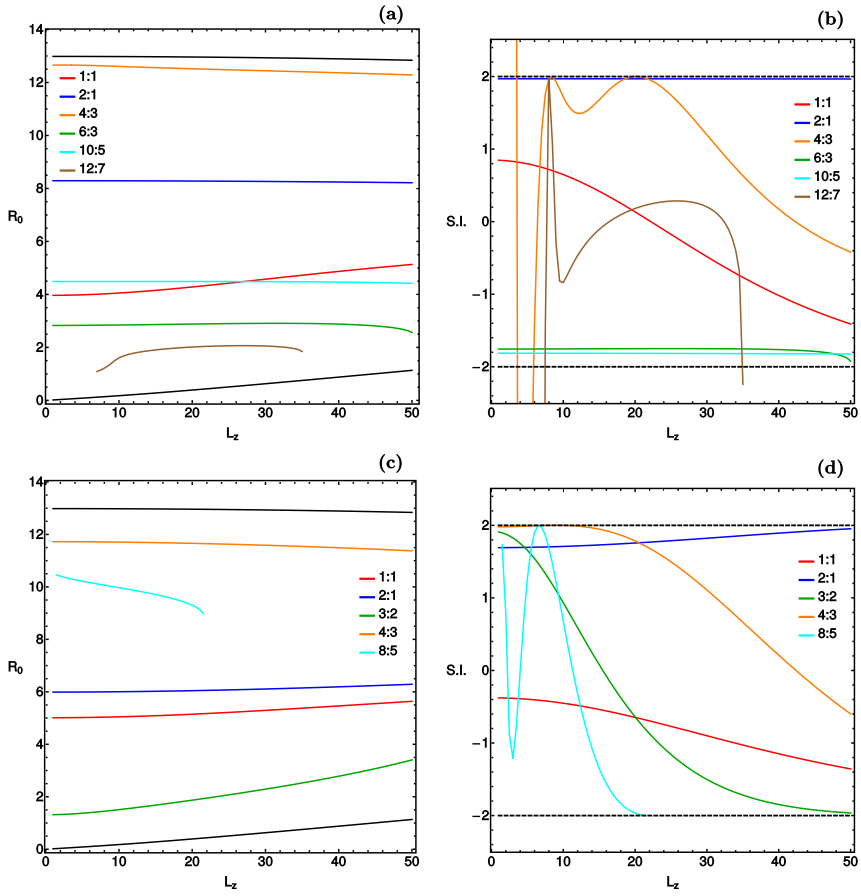

Fig. 9. Evolution of the R coordinate of periodic orbits as a function of the angular momentum $L_{\rm z}$ for the PH models (panel a) and OH models (panel c), and the evolution of the stability index S.I. as function of $L_{\rm z}$ for the PH models (panel b) and OH models (panel d).

4.9. Influence of the angular momentum

One of the most important quantities, which plays a vital role in the nature of star orbits in the meridional plane (R, z), is the angular momentum $L_{\rm z}$. Therefore, it is of paramount significance to investigate how the angular momentum affects the position and the stability of periodic orbits in our PH and OH galaxy models. We let this quantity vary while fixing the values of all the other parameters of our galactic models and integrating orbits in the meridional plane for the set $L_{\rm z} = \{1, 5, 10, ..., 50\}$.

In Fig. 9a we present how the position of periodic orbits in our PH models evolves as a function of the angular momentum. The corresponding stability diagram in panel (b) shows that the 4:3 resonant family becomes unstable in the

interval $1.62 \leq L_z \leq 5.51$. Furthermore, the 12:7 resonant family is unstable for $6.34 \leq L_z \leq 7.12$ and for $34.86 \leq L_z \leq 35.09$, while the same family disappears near the two opposite ends of the range of values of L_z. Panel (c) shows the evolution of the R coordinate of periodic orbits of the OH models as a function of the angular momentum L_z. All resonant families are present in the entire range of values except for the 8:5 resonant family which terminates at $L_z = 21.53$ without first exhibiting any unstable branch.

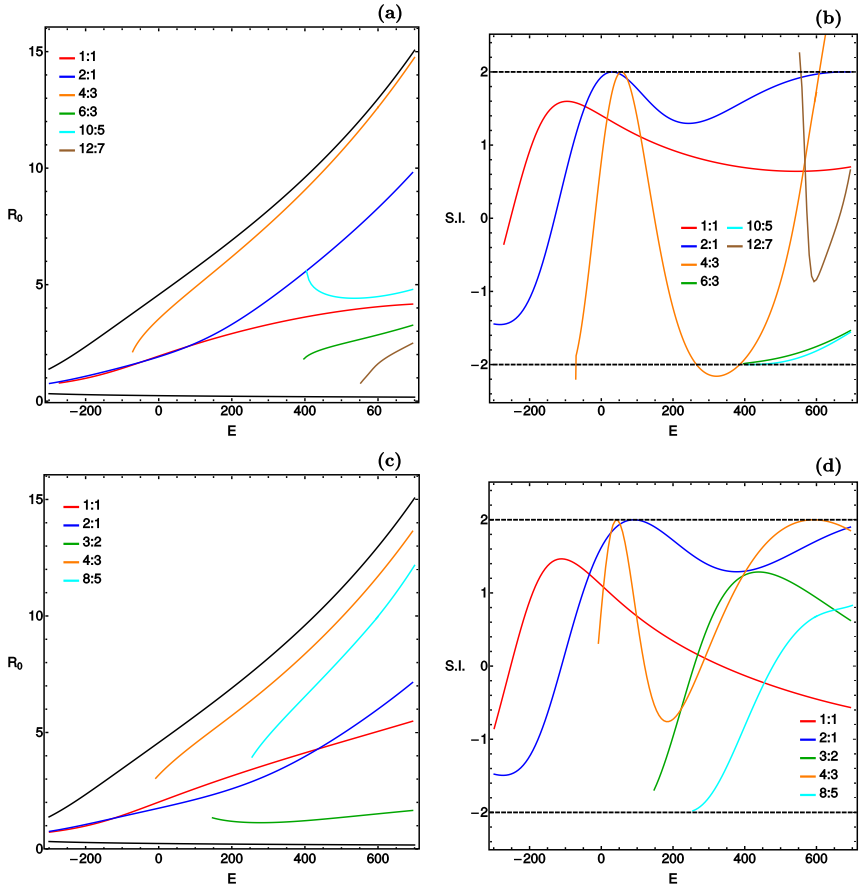

Fig. 10. Evolution of the R coordinate of periodic orbits as a function of the total orbital energy (E) for the PH models (panel a) and OH models (panel c), and the evolution of the stability index S.I. as a function of E for the PH models (panel b) and OH models (panel d).

4.10. Influence of the orbital energy

The last parameter under investigation is the total orbital energy E. To explore how the energy level affects the position and the stability of periodic orbits in our PH and OH galaxy models, we use the normal procedure according to which we let the energy vary while fixing the values of all the other parameters of our galactic models and integrating orbits in the meridional plane for the set $E =$

$\{-300, -200, -100, 0, 100, ..., 700\}$. At this point we should point out that the particular value of the energy determines the maximum possible value of the R coordinate ($R_{\max}$) on the $(R, \dot{R})$ phase plane. The energy values in the above interval result in $1.4 < R_{\max} < 15$.

The evolution of the position of the periodic orbits as a function of the total orbital energy in our PH models is presented in Fig. 10a. We should point out three aspects: (i) for low values of the orbital energy ($E < -100$), which correspond to local motion around the nucleus, only two main resonant families (2:1 and 1:1) survive; (ii) all the secondary resonant families (i.e, 6:3, 10:5 and 12:7) emerge at relatively high energy levels ($E > 400$) which correspond to global motion; (iii) at about $E = 400$ we observe how the 10:5 secondary resonant family bifurcates from the main 2:1 family. In panel (b) of the same figure we present the corresponding stability diagram from which we can deduce the following: (i) the 4:3 resonant family is unstable in the intervals $-71.32 \leq E \leq -70.98$, $265.75 \leq E \leq 385.06$ and $609.12 \leq E \leq 700$; (ii) the 6:3 and 10:5 resonant families terminate at $E = 397.28$ and $E = 404.05$, respectively, without first exhibiting any instability; (iii) the 12:7 resonant family starts at $E = 552.71$ and remains unstable for $552.71 \leq E \leq 553.78$. Panel (c) depicts the evolution of the R coordinate of the periodic orbits as a function of E for the OH models. The structure of the characteristic diagram is quite similar to that discussed earlier in panel (a). The stability diagram given in panel (d) shows that all resonant families are stable. In addition one can see that the 3:2, 4:3 and 8:5 resonant families originate at $E = 147.28$, $E = -8.10$ and $E = 255.41$, respectively.

5. DISCUSSION

We used the composite analytic axially symmetric galactic gravitational model introduced in Paper I in order to reveal the complete network of periodic orbits. Varying the values of all the involved parameters of the dynamical system, as well as the two global isolating integrals of motion, namely the angular momentum and the total orbital energy, we managed to construct detailed and aggregated diagrams showing the evolution of the position (R coordinate) and the stability of the main resonant periodic families of orbits as a function of the variable parameters. Here we should emphasize that this is the first such detailed and systematic numerical investigation regarding the influence of all the dynamical quantities of the system on the position and stability of resonant periodic families.

In order to locate the position and measure the stability of the periodic orbits, we used a highly sensitive numerical routine which has the ability to identify resonant periodic orbits of the type $n : m$, where m and n are the main frequencies of a periodic orbit along the R and z axis, respectively. First, for every variable parameter a range of realistic values was defined. The numerical code begins from the value corresponding to the standard model (SPM and SOM) which is always somewhere inside the main interval and then using a variable step scans all the available interval thus calculating the entire resonant family. Two different cases were investigated for every parameter: (i) the case where the dark matter halo component is prolate and (ii) the case where an oblate dark matter halo is present.

Our numerical computations revealed that all the dynamical quantities affect, more or less, the position as well as the stability of the resonant periodic orbits.

It was observed, however, that for both types of models (PH and OH) the mass of the nucleus, the mass of the disk, the halo flattening parameter, the scale length of the halo, the angular momentum, and the total orbital energy are the most influenced quantities, while the effects of the scale length of the nucleus and that of the horizontal and vertical scale length of the disk are much weaker.

ACKNOWLEDGMENTS. I would like to express my warmest thanks to Dr. Leonid P. Ossipkov (University of Saint Petersburg) for the careful reading the manuscript and for all the apt suggestions and comments that allowed me to improve both the quality and the clarity of the paper.

REFERENCES

Abalakin V. K. 1961, Bull. Inst. Theor. Astron., 8, 173
Abalakin V. K. 1963, Bull. Inst. Theor. Astron., 9, 204
Antonov V. A. 1974, Trans. Astron. Obs. Lenigrad State Univ., 30, 111
Allen C., Santillán A. 1991, Rev. Mex. Astron. Astrof., 22, 255
Belbruno E., Llibre J., Ollé M. 1994, Celest. Mech., 60, 99
Binney J., Tremaine S. 2008, *Galactic Dynamics*, Princeton Univ. Press
Bollt E. M., Lai Y. C., Grebogi C. 1997, Phys. Rev. Lett, 63, 3787
Carlberg R. G., Innanen K. A. 1987, AJ, 94, 666
Carpintero D. D., Aguilar L. A. 1998, MNRAS, 298, 1
Contopoulos G., Barbanis B. 1985, A&A, 153, 44
Contopoulos G., Magnenat P. 1985, Celest. Mech., 37, 387
Contopoulos G., Mertzanides C. 1977, A&A, 61, 477
Contopoulos G., Seimenis J. 1990, A&A, 227, 4
Cvitanović P. 1991, Physica D, 51, 138
Davidchack R. L., Lai Y. C., Bollt E. M., Dhamala M. 2000, Phys. Rev. E, 61, 1353
Devaney R. L. 1989, *An Introduction to Chaotic Dynamical Systems*, 2nd ed., Addison-Wesley Publishing Co.
Deprit A., Henrard J. 1967, AJ, 72, 158
Gómez G., Llibre J., Martínez R., Simó C. 1985, *Station Keeping of Libration Points*, ESOC Conf. 5648/83/D/JS(SC)
Gutzwiller M. C. 1990, *Chaos in Classical and Quantum Mechanics*, Springer Verlag
Henrard J., Lemaitre A. 1986, Celest. Mech., 39, 213
Howell K. C. 1984, Celest. Mech., 32, 53
Karimov S. R., Sokolsky A. G. 1989, Celest. Mech., 46, 335
Lara M., Paláez J. 2002, A&A, 389, 692
Lathrop D. P., Kostelich E. J. 1989, Phys. Rev. A, 40, 4028
Miyamoto W., Nagai R. 1975, PASJ, 27, 533
Ott E. 1993, *Chaos in Dynamical Systems*, Cambridge University Press
Ott E., Grebogi C., Yorke J. A. 1990, Phys. Rev. Lett, 64, 1196
Plumecoq J., Lefranc M. 2000, Physica D, 144, 231

Prendergast K. H. 1982, in *The Riemann Problem*, Lecture Notes in Mathematics, Springer-Verlag, 925, 369

Press H. P., Teukolsky S. A., Vetterling W. T., Flannery B. P. 1992, *Numerical Recipes in FORTRAN 77*, 2nd ed., Cambridge Univ. Press

Scheeres D. J., 1999, in *Hamiltonian Systems with Three or More Degrees of Freedom*, NATO AS I Ser., vol. 533, p. 554

Wood D. 1984, IMA J. Appl. Math., 33, 229

Zotos E. E. 2013, Nonlinear Dynamics, 73, 931

Zotos E. E. 2014, A&A, 563, A19 (Paper I)

Zotos E. E., Carpintero D. D. 2013, CeMDA, 116, 417